Polymer Testing 100 (2021) 107261

Contents lists available at ScienceDirect

Polymer Testing

journal homepage: www.elsevier.com/locate/polytest

Quasi static mechanical study of vacuum bag infused bouligand inspired composites

L. Amorim *, A. Santos, J.P. Nunes, G. Dias, J.C. Viana

IPC – Institute for Polymers and Composites, University of Minho, Guimarães, Portugal

ARTICLE INFO

Keywords:
Carbon fibre
Bouligand architecture
Vacuum bag infusion
Quasi-static testing
FE modelling
Failure mode

ABSTRACT

Three novel Bouligand inspired composites were produced by vacuum bag infusion manufacturing process and their quasi-static mechanical performance were compared to a conventional aircraft laminate. A morphologic/physical study was first conducted for all configurations and their mechanical response under tensile, three-point bending (3-PB) and interlaminar shear strength (ILSS) tests were then evaluated and discussed. No significant number of voids were detected into laminates, however, a rough and poor defined interlaminar region was observed in both Bouligand-like configurations. Under quasi-static mechanical solicitations, and when compared to reference layup, bioinspired configurations have shown similar and 18% higher tensile and flexural modulus. However, the progressive and translaminar failure mode, typically observed in these configurations, led to a lower load bearing capability. Despite presented similar interlaminar resistance than reference, finite element models built have revealed a good correlation between cross-section stress field and failure mode observed experimentally.

1. Introduction

Despite their outstanding in-plane mechanical properties, advanced composite materials still presenting some issues when submitted to out-of-plane or fatigue loading. Under these conditions, they tend to develop internal matrix micro cracks that may propagate across their interlaminar region, compromising the performance of components or even, in the worse scenario, lead to its catastrophic failure.

In order to overcome these problems, in the last decades a close insight over biologic material structures have been seen as potential inspiration for synthetic composites. Especially, Bouligand plywood arrangements [1] have attracted particular attention regarding their similarity to advanced composites and outstanding damage tolerance. They are twisted laminate arrangements found in a large range of crustaceous exoskeletons and hunting weapons [2,3], consisting in unidirectional fibrous plies stacked with small mismatch angle between them, completing a 180° helical rotation along the perpendicular axis to the stacking plan. Fig. 1 shows the particular case of mantis shrimps *Odontodactylus Scyllarus* [4] and their dactyl clubs composed by several Bouligand structures stacked each other providing toughness and avoiding their catastrophic failure during the attack.

Several studies were already carried out in order to mimic these natural helical fibrous arrangements in common synthetic composite systems, such as is the case of the glass or carbon fibres reinforced polymers [4–18]. Most of those studies reported that, under out-of-plane loading conditions, the built Bouligand-like structures outperformed the respective baseline laminates in terms of load bearing capacity and/or damage resistance [5,6,9,10,13,14,16–19]. In order to better understand the mechanical behaviour of those structures under out-of-plane loading conditions, Mencattelli and Pinho [9,10] manufactured carbon fibre reinforced polymers (CFRP) by using very thin plies of unidirectional carbon fibres, which were progressively and continuously stacked varying the fibre orientation angle to investigate a large range of pitch angles (from 2.5° to 45°). They found that the laminate having the lower pitch angle (2.5°) outperform the quasi-isotropic one not only under LVI and compression after impact (CAI) [9] but also in the three-point bending (3-PB) and transversal plate bending tests [10]. Liu and his co-workers carried out several plate bending experiments over Bouligand-like layups with different arrangements and materials [16–19]. They, once again, demonstrated that, in most of the cases, those structures were able to perform better than their quasi-isotropic and cross-ply corresponding laminates and also concluded that

* Corresponding author..
E-mail addresses: luis.amorim@dep.uminho.pt, lamorim@inegi.up.pt (L. Amorim).
URL: http://www.ipc.uminho.pt (L. Amorim).

https://doi.org/10.1016/j.polymertesting.2021.107261
Received 7 December 2020; Received in revised form 24 May 2021; Accepted 30 May 2021
Available online 6 June 2021

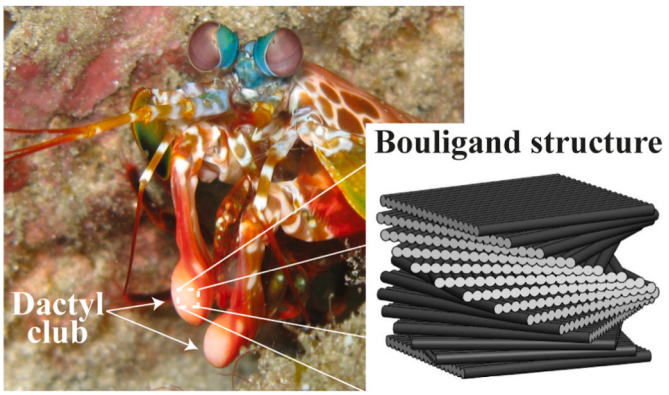

Fig. 1. Mantis shrimps (Odontodactylus Scyllarus) photography [4] and a schematic representation of a Bouligand structure present its dactyl clubs.

optimal inter-ply angle increased with the thickness of plies [17] and lower toughness matrix, whereas fibre toughness seems to play a less important role [19].

Despite the efforts to optimize the suitability of those biologic structural arrangements in advanced composites, only prepreg fibre reinforced polymer (FRP) systems were used in the experimental works found in the literature available. However, the use of other FRP manufacturing technologies where dry fibres are impregnated by a liquid resin, which may cause morphologic and physical changes, can lead to different mechanical behaviours.

In this context and for the first time, three Bouligand inspired and a conventional aircraft laminate were manufactured by vacuum bag infusion in this work to allow comparing their morphologic/physical properties and mechanical behaviours. All those laminates were submitted to tensile, 3-PB and short-beam interlaminar shear strength (ILSS) experimental tests and the obtained results, failure modes and mechanical responses will be presented and discussed exhaustively.

2. Experimental

2.1. Materials, processing and laminates

In this work, all laminates were produced using as a main reinforcement a 150 g/m^2 unidirectional carbon fibre (UDCF) fabric (Dynanotex HS 24/150 DLN2) from G. ANGELONI s.r.l.. According to the provider, Dynanotex is a unidirectional carbon fibres tissues manufacturing system that consists of two layers of PAN carbon fibres (Grafil 24K 1600 dtex) from Mitsubishi, perfectly aligned and bonded together by a central polyester fibre weft thread with a resin compatible adhesive.

As matrix system was used a low viscosity (610 mPa s) bicomponent epoxy resin. Specifically designed from Sika® for infusion process, 70% of Biresin® CR83 neat resin was mix with 30% of CH83-6 hardener and degassed during 20 min before infusion.

The fibre fabrics were first cut in rectangles of 600 × 500 (mm) by using a 1 kW laser cutting machine. The different ply angles were previously set on the control operator command of the laser machine. The final cut fabrics were carefully stacked up manually layer-by-layer under glass flat mould. All laminates were manufactured by vacuum bag infusion at room temperature and, afterward, post-cured inside an oven at 70 °C for 8 h.

Four different CFRP layup arrangements (Fig. 2) were manufactured in this work, namely, a standard aircraft (LS) and three bioinspired laminates (HL, HL_S and HYB). Similar to LS laminate, both Bouligand-like layup arrangements (HL and HL_S) were composed by 28 layers of 150 g/m^2 UDCF fabric, while HYB configuration was composed by 14 of those main layers and 42 UDCF thinner 50 g/m^2 layers, for a total of 56 UDCF plies.

Table 1 describes the stack sequences used in the different laminates as well as the number and type of UDCF layers used in each one.

In both Bouligand-like configurations (HL and HL_S) was used an inter-ply angle of 13.3°, however, while HL presents an antisymmetric arrangement ([B]≠0), HL_S was designed with a midplane symmetric architecture ([B] = 0) to avoid physical in-plane twisting of the laminate after curing. Finally, the HYB laminate was specially designed to present a hybrid structural solution that could represent a compromise between the LS and bioinspired ones. One of the main reasons for the growing interest in Bouligand-like structures leads on their outperformance under out-of-plan loading conditions essentially conferred by their unique helical plywood architecture and small transition angle between plies. Therefore, the methodology behind HYB laminate structural design consisted in to keep the main stacking configuration of LS laminate, however, this time, symmetric just once about mid-thickness ($[0/45/90/-45/45/-45/0]_S$), consisting in 14 layers of 150 g/m^2 UDCF, called since from now on main layers. Then, a sub-laminate (α^i) composed by 3 thinner 50 g/m^2 Dynanotex HS 15/50 SLN2 UDCF layers, also from G. ANGELONI s.r.l., with a constant pitch angle were interleaved into each interlaminar region in order to create four smooth and constant translaminar rotation between the main 150 g/m^2 plies. Thus, the angle between the three thinner plies used in the interleaved sub-laminates depends on the angle formed between the two main adjacent layers that they are placed. When two adjacent main plies were

Table 1
Laminates' configuration.

Laminate	N° of layers		Stacking Sequence
	150 g/m^2	50 g/m^2	
LS	28	–	$[0/45/90/-45/45/-45/0]_{2S}$
HL	28	–	[0/13.3/26.6/ … /360]
HL_S	28	–	$[0/13.3/26.6/ \ldots /173.3]_S$
HYB	14	42	$[0/\alpha^1/45/\alpha^2/90/\alpha^3/-45/\alpha^4/45/\alpha^5/-45/\alpha^6/0/\alpha^7]_S$

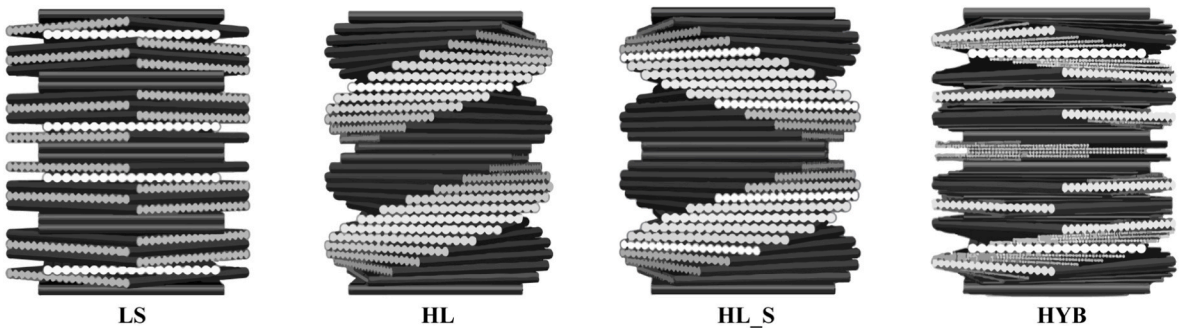

Fig. 2. Laminates schematic representation.

stacked with a 45° inter-ply angle, an angle of 11,25° was used between the sub-laminate plies (45°/4 interfaces) and, for main plies making 90° angles between them, a 22.5° angle was used as a sub-laminate pitch angle (90°/4 interfaces).

Therefore, and in more detail, considering the two HYB adjacent main plies oriented at 0° and 45° (which makes a 45° between them), three 50 g/m^2 thinner UDCF layers were included between them, the so-called sub-laminate α^1, which generate four new interlaminar regions with inter-ply angle of 11.25°, as mentioned above. This methodology was similarly repeated for the main adjacent plies oriented at 45°/90°, 90°/-45°and −45°/0°, generating sub-laminates α^2, α^3 and α^6, respectively. For the main adjacent plies stacked with an inter-ply angle of 90°, namely −45/45 and 45/-45, the sub-laminates' pitch angle was 22.5°, generating sub-laminate α^4 and α^5, respectively. Finally, to provide symmetry to the whole laminate and an interlaminar transition region between main plies, in the 0°/0° adjacent main plies particular case, two α^7 sub-laminates were interleaved symmetrically, with an interplay angle of 30°.

The seven sub-laminates used to interleaf HYB main layers were:

α^1 = [11.25/22.5/33.75];
α^2 = [56.25/67.5/78.75];
α^3 = [-78.75/-67.5/-56.25];
α^4 = [-22.5/0/22.5];
α_5 = -α^4;
α^6 = [-33.75/-22.5/-11.25];
α^7 = [30/60/90].

Despite to be manufactured using the same technology used to produce the main 150 g/m^2 UDCF fabric (Dynanotex HS 24/150 DLN2) described above, this 50 g/m^2 unidirectional carbon fibre fabric, are produced from a single carbon fibre layer, regarding the thin thickness required, therefore, weft threads are exposed on the UDCF tissue outer surface.

2.2. Testing

The testing campaign was divided in two main topics: i) laminates physical and morphological characterisation, ii) quasi-static mechanical performance, namely under tensile, 3-PB and ILSS tests. All samples were carefully marked on each laminate panel, and then cut using a low-speed diamond circular saw with water cooling, to minimise cutting damages in the edges.

2.2.1. Laminates' characterisation

Laminates' characterisation was conducted taking into account three different aspects: a) thickness, b) fibre volume fraction and c) morphology.

a) To assess the laminates thickness, all tensile, 3-PB and ILSS samples were measured in three different locations using a calliper rule.
b) Laminates' fibre volume fraction evaluation was divided in three phases. First, according with ISO 1183 standard procedures, the specific mass of each laminate components raw material was determined, then, using a thermogravimetric analysis (TGA) device (Q500 from TA Instruments USA), the composites and their row material components residual mass were evaluated. Finally, fibre volume fraction of each laminate was determined. A detailed description of laminates fibre volume fraction determination may be founded in the supplementary material appendix A.
c) For the morphological analysis, three samples of each laminate were embedded by an epoxy resin in a small mould and allowed to cure during 24 h, then samples were carefully polished and covered with a thin layer of gold before being observed under scanning electron microscope (SEM) to evaluate matrix/fibres adhesion and presence of void spots on them.

2.2.2. Tensile tests

In-plane mechanical properties were determined by tensile mechanical tests. A set of five tabbed 25 × 250 (mm) specimens of each laminate, with the 0° plies orientated in loading direction, were tested following ASTM D3039 standard procedures in a 100 kN load cell SHIMADZU® AG-X universal testing equipment using a 2 mm/min loading speed. An axial clip-on extensometer was used to measure the specimen longitudinal deformation up to 0.004, then the test was stopped to remove the extensometer and, restarted again until the specimen failure. As the extensometer was removed during tests, no accurate failure strain values could be obtained. The longitudinal Young's modulus (E) was determined between the strains of 0.001 and 0.003 measured by the extensometer and the maximum stress (σ) obtained from the loading data recorded by the testing machine. Tests were finished only when the catastrophic failure occurred. Finally, experimental laminates' Young's moduli were compared to those theoretically calculated using Classical Lamination Theory (CLT) [20]. Lamina engineering constants used to perform the calculations were first experimentally obtained and are presented in Table 2.

2.2.3. Three-point bending (3-PB) tests

Regarding flexural properties, all laminates were submitted to 3-PB tests according with ASTM D7264 standard. Tests were carried out in the SHIMADZU® AG-X universal testing machine with a loading cell of 50 kN at a testing speed of 1 mm/min. Five 170 × 13 (mm) specimens of each laminate, with the 0° plies oriented perpendicular to loading nose, were been tested to determine their maximum outer surface stress ($\sigma_{out.\ surf.}$) and flexural modulus ($E_{flex.}$) from the testing data. The flexural modulus was determined between the 0.001 and 0.003 flexural strain. Each test was concluded after a significant load drop followed by a visible failure occurred. Once again, laminates' experimental $E_{flex.}$ were compared to theoretical results computed using CLT [20].

2.2.4. Interlaminar shear strength (ILSS) tests

ILSS tests were performed in accordance with ISO 14130 standard to evaluate and compare the interlaminar shear strength among the different laminates. All experiments were performed in a 50 kN SHIMADZU® AG-X universal testing machine at a loading speed of 1 mm/min using five specimens with dimensions of 40 × 20 (mm), having the 0° plies oriented perpendicular to loading nose. The first failure was determined in each laminate when the load started to fall on the load/displacement curve.

3. Results

3.1. Laminate characterization

As may be seen in Table 3, while the LS, HL and HL_S laminates presented very similar thicknesses and fibre volume fractions with values around 3.8 mm and 64%, respectively, the HYB laminate has shown to be thicker and having lower fibre volume content, approximately 11% and 14%, respectively, when compared the other laminates.

Fig. 3(a) presents a 300 times magnified SEM microphotograph where is possible to observe the main different material phases detected in all laminates. It allows clearly identify: i) the UD carbon fibre, ii) the Biresin® CR83 matrix system used to impregnate those fibres by vacuum bag infusion, iii) the weft thread and adhesive resin used to keep the

Table 2
Experimental properties obtained for the unidirectional lamina.

E_{11} (GPa)	$E_{22} = E_{33}$ (GPa)	$G_{12} = G_{13} = G_{23}$ (GPa)	υ_{12}	$\upsilon_{13} = \upsilon_{23}$
99.784 ± 9.375	6.454 ± 0.087	2.964 ± 0.051	0.32 ± 0.04	0.017 ± 0.001

Table 3
Laminates' average and (±) stander deviation thickness and fibre volume fraction.

Laminate	Thickness	Fibre volume fraction
	mm	%
LS	3.82 ± 0.05	63.3 ± 1.2
HL	3.77 ± 0.08	65.1 ± 0.8
HL_S	3.79 ± 0.08	63.1 ± 0.4
HYB	4.20 ± 0.17	55.3 ± 1.1

carbon fibres bonded to the weft thread and aligned in the same direction during manufacturing process of fabrics. Moreover, red dotted areas depicted in the figure highlight laminate interlaminar regions.

Fig. 3 (b) shows a representative image (magnification: 5000 ×) demonstrating the good fibre/matrix adhesion that was obtained in all laminates. Finally, Fig. 3 (c) shows, at the magnification of 5000 times, the negligible number of small voids found inside the HL laminate.

3.2. Quasi static mechanical test results: tensile, 3-PB and ILSS

Table 4summarises the average results obtained for the tensile Young's modulus (E) and maximum stress (σ), long 3-PB flexural modulus ($E_{flex.}$) and maximum outer surface stress ($\sigma_{out.surf.}$) and maximum short-beam interlaminar shear stress (τ_{13}).

3.2.1. Tensile tests results

Under tensile tests (see Table 4), only whole HL experimental samples have presented valid failures, while one HL_S specimen, two LS and all HYB ones failed at tab's regions. Thus, only the valid specimens were considered to determine the maximum failure stress (σ) of laminates. Since a clip-on extensometer was used for all experiments, all data tests were, however, considered to calculate the tensile elastic modulus (E) of laminates.

Tests did not reveal significant differences between the Young's moduli (E) of laminates, with all of them presenting a similar value around 40 GPa. However, HL and HL_S laminates have shown to fail at 26% and 37% less tensile stress than the LS one, respectively. Moreover, despite have failed in tab's regions, HYB tensile failure stress has shown to be at least slightly higher than HL and HL_S configurations.

Table 4
Theoretical (CLT) and experimental (Exp.) average (±standard deviation) results of: tensile Young's modulus (E) and maximum stress (σ); long 3-PB flexural modulus ($E_{flex.}$) and maximum outer surface stress ($\sigma_{out.surf.}$); short-beam interlaminar maximum 13 shear stress (τ_{13}).

	Tensile			3-PB			ILSS
	E		σ	$E_{flex.}$		$\sigma_{out.surf.}$	τ_{13}
	GPa		MPa	GPa		MPa	MPa
	CLT	Exp.		CLT	Exp.		Exp.
LS	40.4	43.8 ± 3.0	540 ± 64	42.3	38.2 ± 1.3	462 ± 26	18.8 ± 0.9
HL	39.9	39.8 ± 0.8	399 ± 42	50.4	42.5 ± 0.5	362 ± 20	19.2 ± 0.9
HL_S	39.9	40.8 ± 2.6	339 ± 28	42.5	44.9 ± 0.8	372 ± 17	16,9 ± 1.1
HYB	44.0	39.9 ± 1.8	>409	43.1	36.7 ± 1.6	428 ± 17	25.1 ± 1.0

3.2.2. 3-PB tests results

The results obtained under 3-PB tests (see Table 4) show that HL and HL_S configurations present 11% and 18% higher flexural modulus ($E_{flex.}$) than the standard LS laminate, respectively, while HYB layup revealed to have a slight lower flexural modulus, around 4%, than this last configuration of reference. Results also revealed that LS layup withstands larger tensile stress than the other configurations, which have shown 22%, 19% and 7% less values in case of the HL, HL_S and HYB laminates, respectively.

Fig. 4 a) presents the load vs displacement curves obtained from the 3-PB tests made on each laminate.

3.2.3. ILSS tests results

As may be seen on Table 4, HYB laminate presented the highest maximum apparent interlaminar shear stress (τ_{13}) at first failure (~34% higher average value than LS laminate), while the HL one demonstrated to have only a slightly higher value (~2%) than the standard LS composite. On the other hand, the HL_S laminate has shown the lowest interlaminar global resistance, around 11% less than LS layup arrangement.

Fig. 4 b) shows load vs displacement curves obtained experimentally from ILSS tests.

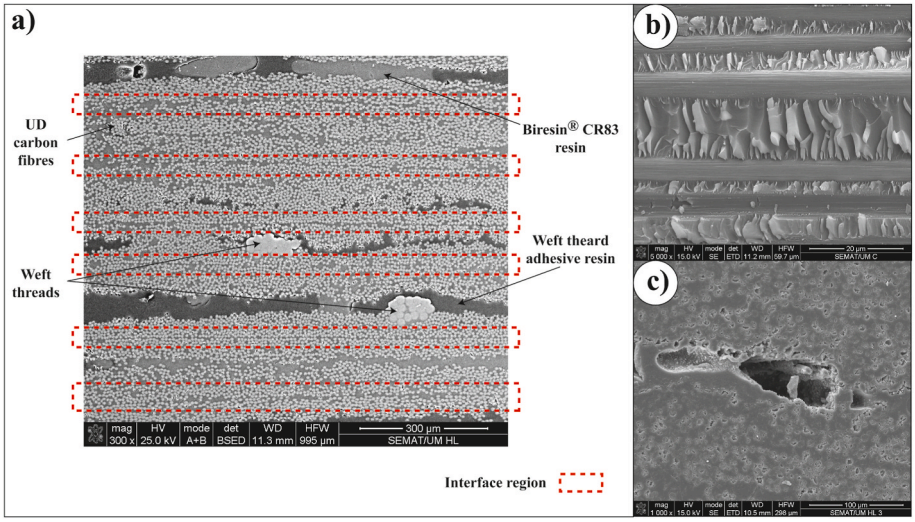

Fig. 3. Morphologic analysis under SEM. a) Interlaminar regions (red dotted) and the different regions in laminates (300 ×); b) Fibre/matrix adhesion (5000 ×); c) Example a void spot found in the HL laminate (1000 ×). (For interpretation of the references to colour in this figure legend, the reader is referred to the Web version of this article.)

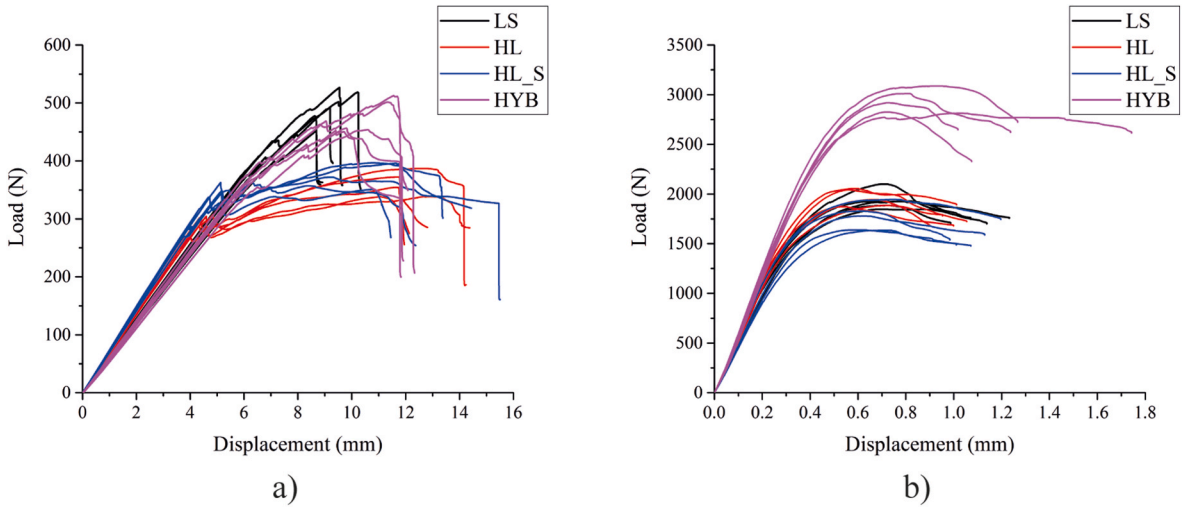

Fig. 4. a) 3-PB and b) ILSS load vs displacement curves of LS, HL, HL_S and HYB specimens.

4. Discussion

4.1. Bouligand-like structures produced by vacuum bag infusion process

Fig. 5 shows a representative cross-section SEM image of each laminate obtained during their morphologic inspection.

As it may be seen in this figure, a substantial number of resin pockets were formed during the manufacturing process. The 300× magnified observation of laminates cross-sections shows that these rich resin spots are apparently mostly deposited in the gaps created by the weft threads used for keeping carbon fibres correctly aligned. It's possible to distinguish the darker phase present on these resin pockets, corresponding to adhesive used to keep the UD carbon fibres and weft threads together in the tissue manufacturing process, from the grey region filled by the epoxy Biresin® CR83 matrix used in the vacuum bag infusion. It's also important to note that the weft thread fibres have a much higher diameter than carbon fibres and appear in more number in HYB laminate (Fig. 5 d) due to the higher number of layers that it is made of (14 + 42* layers, see Table 1), which justify the highest amount of resin pockets present in this laminate when compared to the other ones and, consequently, also its higher thickness and lower carbon fibre volume content.

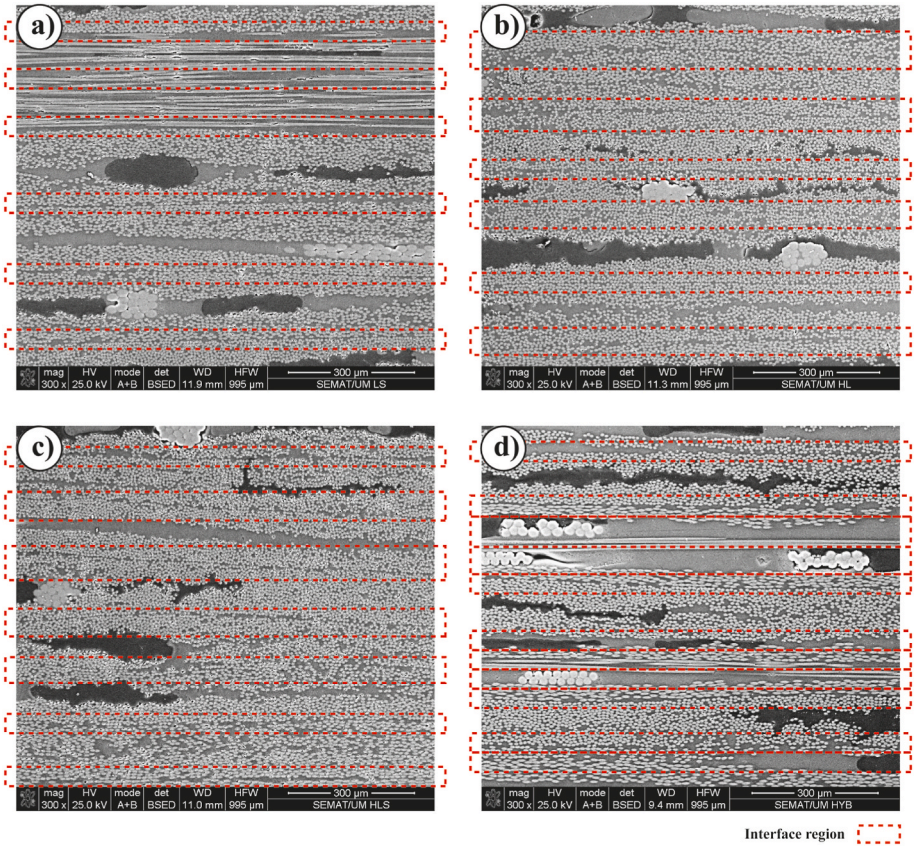

Fig. 5. Representative cross-section morphology of a) LS, b) HL, c) HL_S and d) HYB laminates magnified 300 times in SEM.

In Fig. 5 (b and c) is also possible to see the rough and often poorly defined interlaminar regions (red dotted areas) typically observed on helical laminates (HL and HL_S). Much better defined interlaminar regions were observed in LS samples (see Fig. 5 a), despite some roughness that may be seen. On the other hand, HYB's ply interfaces are thicker and much well-defined due to the already mentioned resin pockets formed around weft threads (see Fig. 5 d).

The cross-section morphologic analysis undertaken revealed, in some cases, rough and disperse interlaminar regions, contrasting with microscopic observations of those regions made by other researches that worked with CRFP prepreg systems [21–23]. This seems to result from the out-of-plane dry fibres rearrangement during the compaction stage, which occurs before resin impregnation in the vacuum bag infusion. The phenomenon becomes more evident when smaller mismatch angles between layers were used, as shown in Fig. 5b) and c), where fibres partially fill the gaps between each other, than when greater angles were applied between layers, i.e. LS configuration (see Fig. 5 d)) where less interlaminar roughness may be observed. Such rough interlaminar interface, especially observed in both Bouligand-like configurations (i.e. in HL and HL_S) may improve interlaminar toughness and crack propagation resistance as it was found in the previous works [11,24]. Nevertheless, the high interlaminar interference caused by the infusion moulding compaction phase can generate difficulties to the resin flow during manufacturing process and may explain the small number of small voids found in HL laminate (Fig. 3 c).

4.2. Influence of ply orientation on laminate failure mode

Figs. 6–9 show representative magnified images captured under optical microscope from already tested specimens of LS, HL, HL_S and HYB laminates, respectively. Figs. 6–8 present the tensile, 3-PB and ILSS specimens of the LS, HL, HL_S laminates, while in Fig. 9 only presents the 3-PB and ILLS specimens of the HYB laminate. The colour bar on each image identifies the ply orientation angles across laminate thickness. Significant damages observed are pointed by white arrows and red arrows that indicate damages around weft threads, while yellow dotted lines identify visible failure trajectories. Moreover, bending load on images referring to 3-PB and ILSS test was always applied on specimen top surface that may be seen on figures.

In Figs. 6–8 a) show typical images of the tensile failure of LS, HL and HL_S layups, respectively. As previously mentioned, all HYB tensile specimens were kept out from this analysis because they failed in the tabs and weren't considered valid.

As may be seen in Fig. 6 a), LS tensile specimens presented an abrupt and catastrophic failure, without signs of a pattern or a progressive crack propagation. By the contrary, in both helical laminates, HL and HL_S, the failure seemed to be progressive following fibres orientation, as it is highlighted by yellow dotted lines in Figs. 7 and 8 a). While in the HL layup (Fig. 7 a)) the double Bouligand arrangement leaded to a clear antisymmetric twisting crack propagation, the HL_S laminate (Fig. 8 a)) has shown a symmetric failure about specimen's mid-plane following along fibres orientation.

Under the 3-PB tests, LS laminate (see Fig. 6 b)) has shown clear catastrophic compression failures surrounded by several delaminations at the sample compression side (top side on image), while only a small number of delaminations were observed at the side submitted to tensile loads (bottom side on image). As may be seen in the figure, some of those delaminations were formed on weft thread regions (pointed by red arrows), which suggests that the larger diameter of the polyester fibres and the resin pockets associated to those areas may induce the crack initiation.

Figs. 7 and 8 b) show the characteristic 3-PB failure mode of HL and HL_S configurations, respectively. Both laminates presented twist failure mode, along the fibres' direction, at the specimen's compression and tensile sides. As it happened in the tensile tests, the double helical Bouligand HL layup leaded to an antisymmetric twisted crack propagation across specimen's thickness (Fig. 7 b), while HL_S laminate presented a symmetrical failure along its fibrous laminar arrangement (Fig. 8 b). Besides those main failure mode trends (highlighted by yellow dotted lines in the images), some crack branching was also observed in both laminates, that in some cases leaded to an extensive delamination. In both cases and as well as happened in LS laminates, the weft threads and resin pockets formed around them seem to have been responsible for the development of crack branches and delaminations in the composite layup.

The inclusion of thinner layers for smoothing the pitch transition angle between layers induced an apparent twist failure mode in the HYB laminates submitted to 3-PB tests (Fig. 9 a). Apart from two main symmetric helical failures in compression and tensile side, several delaminations, sometimes extensive, were observed, being most of them near weft thread fibres and throughout resin rich pockets formed by them.

Under interlaminar shear stress conditions (ILSS tests), as may be seen in Fig. 6 c), LS configuration presented delaminations between (+) or (−) 45° and 90° direction plies in the specimen's compression and tensile sides. As may be seen from Figs. 7 and 8 c), both Bouligand-like

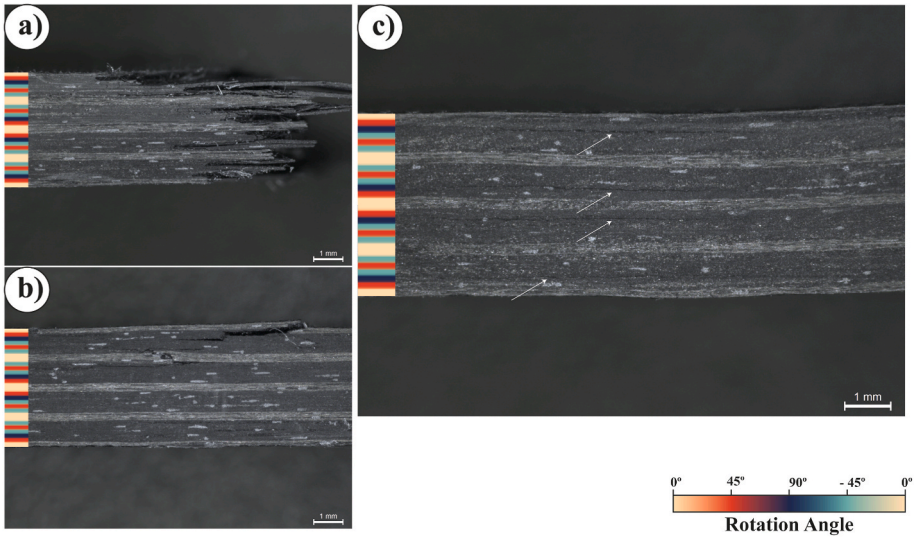

Fig. 6. LS laminate failure mode under a) tensile, b) 3-PB and c) ILSS tests.

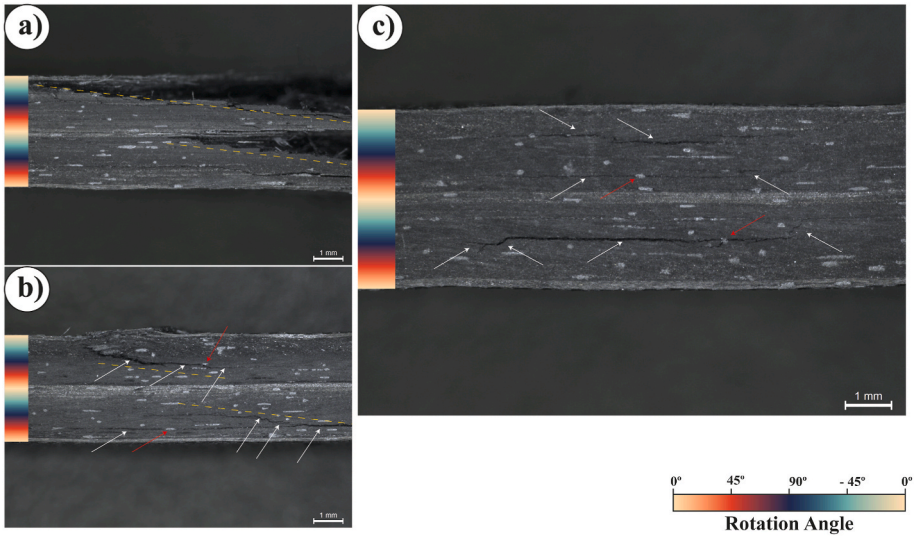

Fig. 7. HL laminate failure mode under a) tensile, b) 3-PB and c) ILSS tests.

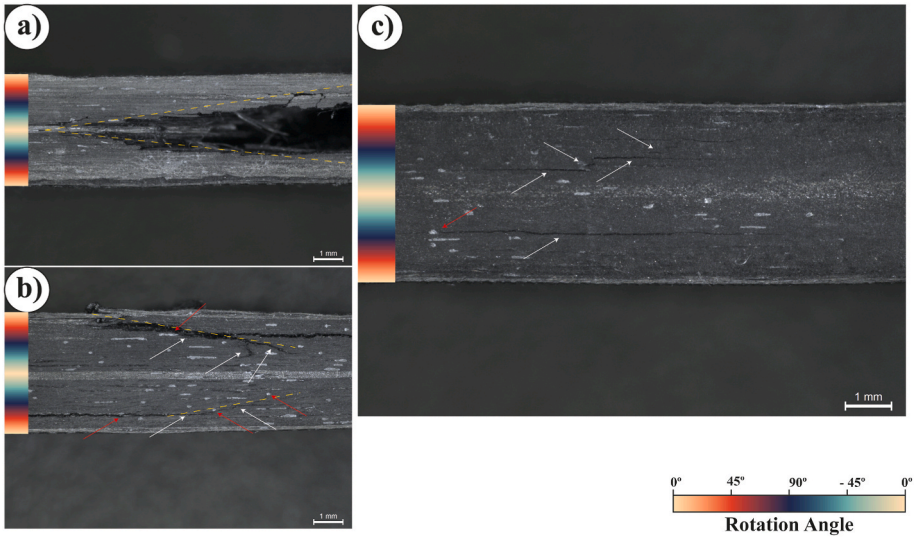

Fig. 8. HL_S laminate failure mode under a) tensile, b) 3-PB and c) ILSS tests.

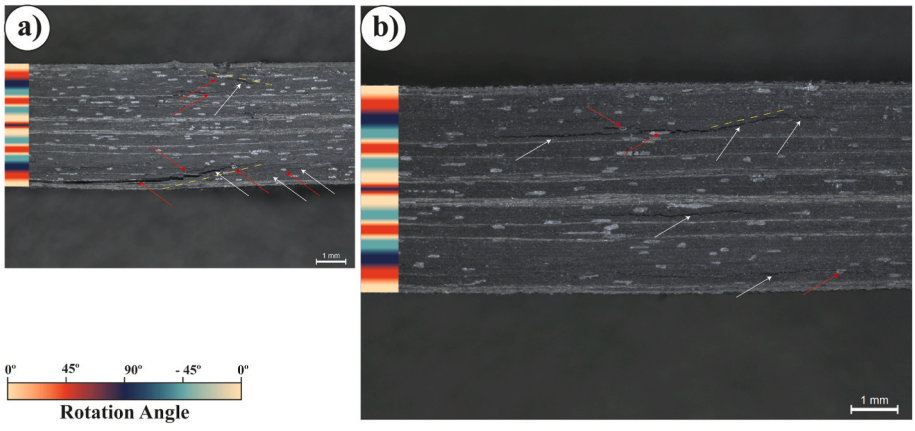

Fig. 9. HYB laminate failure mode under a) 3-PB and b) ILSS tests.

laminates presented a main characteristic failure, composed by two extensive cracks between 90° and −45° plies that at some point jump for other plies in a branched or single translaminar way.

Particularly in HL specimens, small delaminations were also often observed in compression side (top side on image), near their mid-plane (Fig. 7 c). This is in agreement with observations made recently by Ouyang et al. [25] where interlaminar shear stresses, in Bouligand-like laminates, were found to onset failures in several layers simultaneously, leading to a progressive and twisted sub critical crack propagation.

On the other hand, more diffused failure modes were observed in HYB laminates (Fig. 9 b). In the compression side (top side on image), a twist translaminar failure was often observed, while several delaminations were observed in the tensile side (bottom side on image), mostly near the −45° and +45° main layers located closer to the mid-plane and laminate bottom, respectively. However, cracks close weft threads and throughout their resin pockets appeared more often in this layup.

The failure modes resulting from the quasi-static tests made in the several studied composites, suggest that the smooth angle transition between plies on both Bouligand-like and HYB layups, has led to a much progressive twisted failure modes in contrast with the catastrophic failures observed in LS laminates. The smooth and progressive failure mode observed in all bioinspired laminates seems not be only induced by the soft reduction in stiffness from layer to layer, but mostly by fibres orientation which drives crack front across interplay region, as it has been suggested by the work carried out by Suksangpanya et al. [8,26].

4.2.1. *ILSS finite elements elastic model*

Regarding the complex shear stresses field (τ_{13}) developed in the cross-section of specimens under ILSS experiments and to better understand the failure mode of each configuration under these conditions, four finite elements elastic models were built using a commercial ABAQUS® software. The material engineering constraints assigned to the lamina are presented in Table 2.

Both supports and loading nose components were modelled as discrete rigid parts, according to the geometries used in the experimental tests made accordingly to ISO 14130 standard. Each laminate 40 × 20 × 4 (mm) coupon was built as a solid elastic part and, after mesh convergence study to ensure a realistic representation of the experimental elastic stage, 0.1 mm standard linear cubic C3D8R elements across laminate's thickness were used in the loading region. Laminate specimens were simply supported over support components and the loading nose was submitted to a 0.5 mm displacement.

4.2.1.1. ILSS finite elements elastic model results. Fig. 10 shows three-dimensional distribution of τ_{13}, while in Fig. 11 are depicted the projection of its intensity on the cross-section of each layup configurations Width dimension of each model was considered between 0 and 1 and τ_{13}

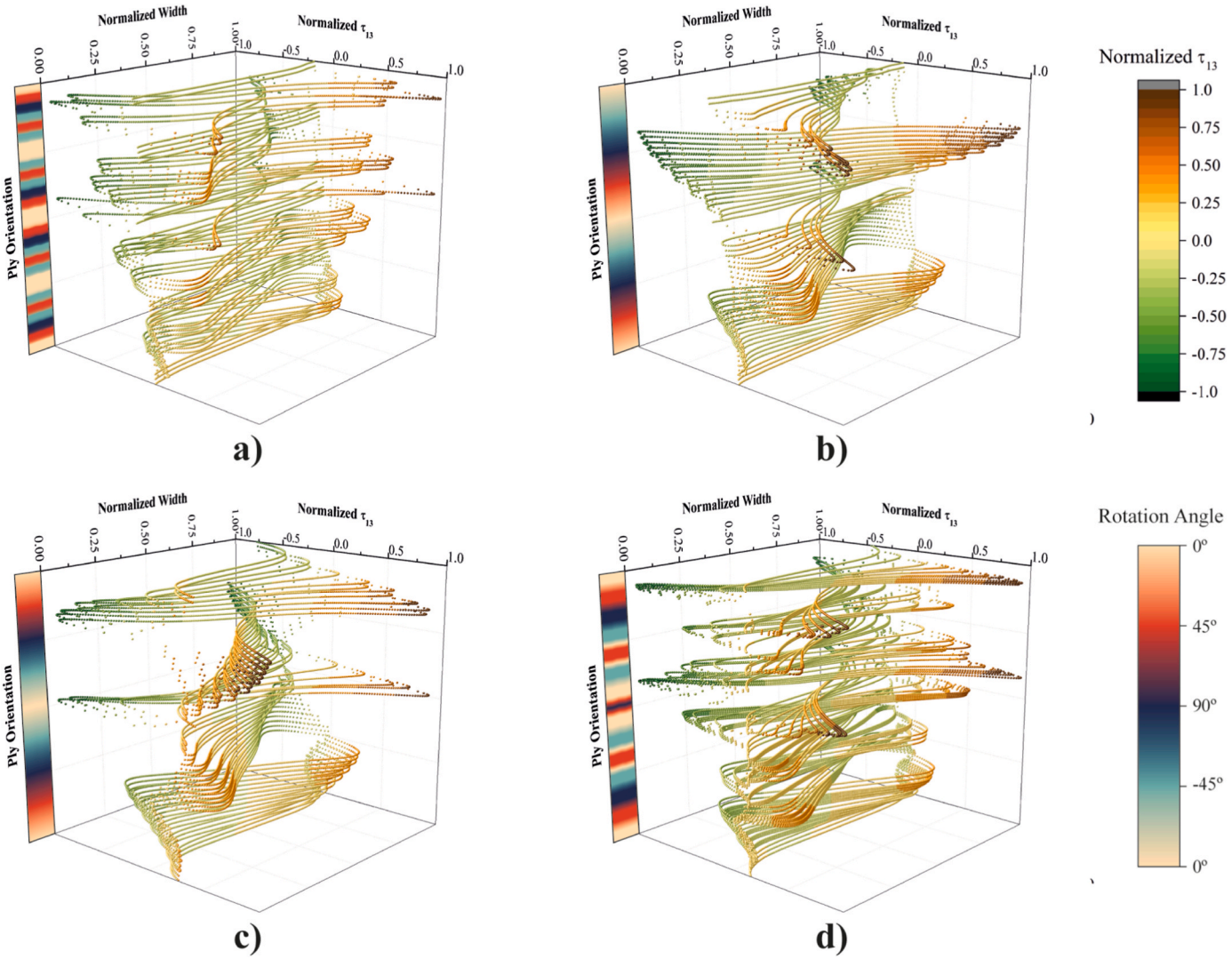

Fig. 10. Three-dimensional τ_{13} distribution on a) LS, b) HL, c) HL_S and d) HYB cross-section.

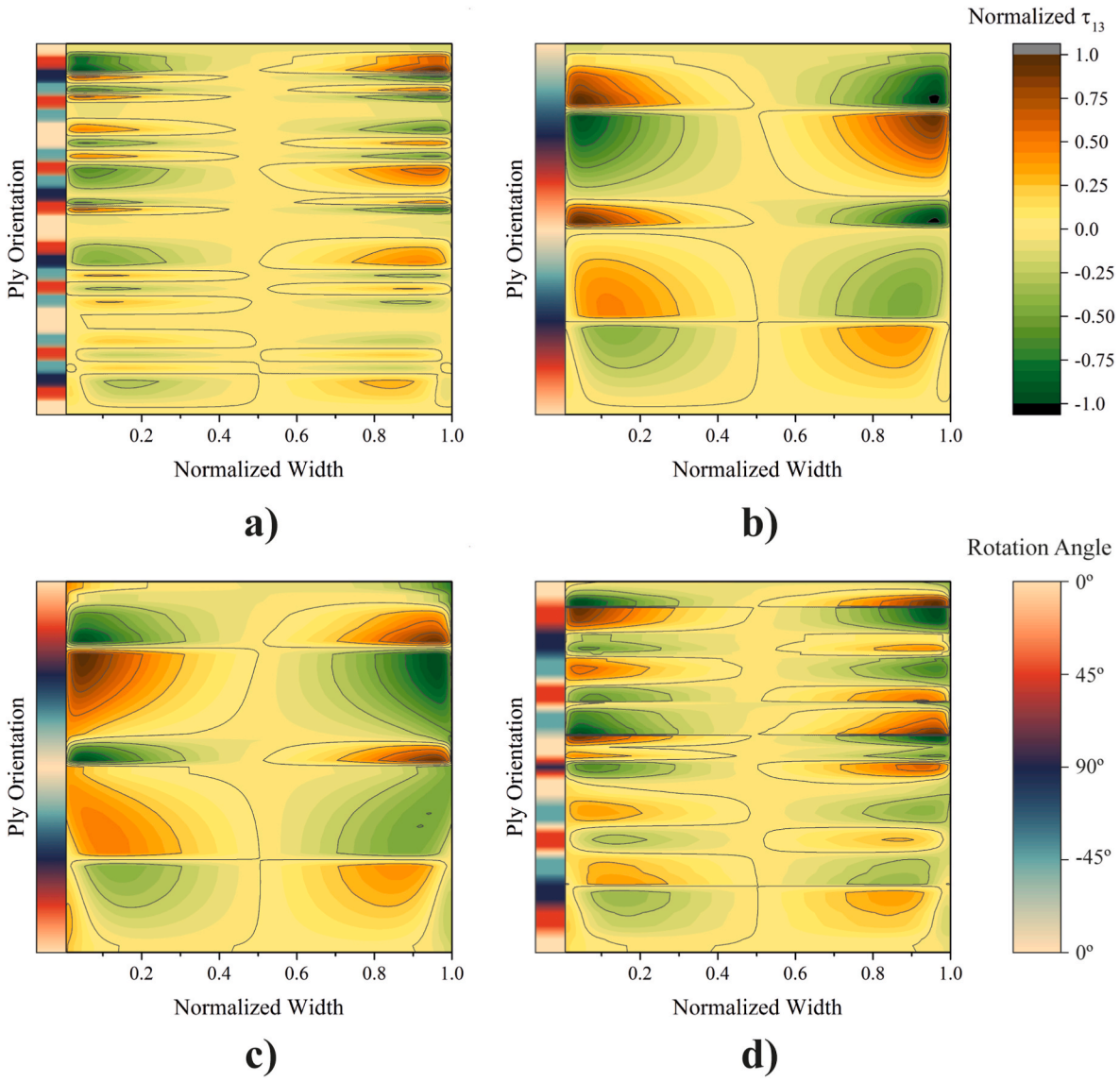

Fig. 11. Projection of τ_{13} intensity on a) LS, b) HL, c) HL_S and d) HYB cross-section.

intensity was normalized to its maximum and minimum of each configuration. The top-right colour bar in both figures classifies stresses intensity, while the bottom-right one identifies plies orientation across specimen's thickness.

From Fig. 10, may be seen a soft τ_{13} transition along the width of each ply, reaching their maximum and minimum close to specimen's edges. However, from ply to ply, this transition has shown to be dependent on plies orientation and may be more abrupt when the mismatch angle is higher. This is particularly evident in Fig. 10 a), where the orientation between plies of LS configuration is larger. On the other hand, in bio-inspired layups this transition tends to be softer, following through the thickness plies orientation (Fig. 10 b to d). Although, when plies are orientated close to a certain angle, an abrupt change in stresses intensity is observed followed by a reset of another helical τ_{13} distribution trend.

From the τ_{13} projection field presented in Fig. 11, is possible to see that stresses are more intense in specimen compression side than in tensile side for all laminates. From the figures is also possible to see that those outmost stresses are more intense, and roughly symmetric about the middle-width, in specimen's edges than in the middle of their cross-section.

The τ_{13} projection of LS layup model results (Fig. 11 a), shows severe changes of stress intensity in some interlaminar regions, although a larger field of similar stresses appears nearby 90° plies followed by a smaller drastic chance in stress intensity. This is in agreement with the location of delamination observed after the ILSS experiments (Fig. 5 c). On the other hand, bioinspired layup model results (Fig. 11 b to d), have demonstrated a smoothest transition in stress intensities when compared to LS results. This was particularly evident for HL and HL_S, in Fig. 11b) and c), respectively, where a constant pitch angle between plies was imposed. However, two particular severe changes in stress intensities may be seen in specimen compression and tensile side of both configurations. Once again, these results are un good agreement with the location of the main failures observed in Figs. 7 and 8 c), moreover the translaminar crack propagation also observed in those figures, seem to follow the stress distribution observe in Fig. 10b) and c). Despite the smoothest transition in stresses between plies observed in HYB model results (Fig. 11 d), when compared to LS ones, several abrupt changes were also detected. However, in this case, despite the translaminar crack propagation experimentally observed (Fig. 9 b)) may be related to the smooth helical stress distribution obtained in the model (Fig. 10 d)), no significant correlation can be done between interlaminar abrupt transitions that have been seen in model results (Fig. 11 d)) and the main failure modes observed in ILSS tests. As it has been mentioned in section

4.2, the high number of weft threads seem to induce cracks initiation leading that then propagate following the stress fields or connecting weft threads throughout the resin pockets.

4.3. Plies' orientation rule on laminates mechanical response

On the previews chapter we discuss how fibres orientation on different laminate architectures could lead to such damage or failure mode mechanisms, now we are going to take a look at fibres orientation rule on mechanical response of each layup arrangement.

Under unidirectional tensile loading conditions all laminates seemed to present similar Young's moduli (Table 4), however, both Bouligand-like HL and HL_S layups have shown a significant reduction of their maximum tensile stress. It seems that, for lower deformations, the small rotation angle between plies of those laminates allows to withstand similar loads as the conventional LS configuration. However, the lower number of fibres orientated on loading direction (Table 1) and progressive failure mechanism observed on both helical configurations (Figs. 7 and 8 a)) leaded to a reduction of their load bearing capability, when compared to LS laminate.

Under 3-PB experiments, despite all specimens had the outer layers orientated with the span direction (0° direction layers), both Bouligand-like laminates have demonstrated higher flexural moduli than LS and HYB configurations. This superior bending stiffness is justified by the lager number of fibres orientated between 0° and 90° on the outer layers when compared to LS configuration, which contributes to a larger stiffness in bending direction. On the other hand, for HYB layup, the lowest flexural modulus is certainly related to the lower fibre volume fraction (Table 3).

Fig. 4 a) presents 3-PB load vs displacement curves of each laminate configuration. As may be seen in the chart, LS specimens presented the highest load bearing capability, followed by HYB and then, with similar behaviour, HL and HL_S layup specimens. The curves also revealed a similar and superior flexural modulus (linear elastic response observed in the first stage of the curves) of HL and HL_S configurations, followed by LS and HBY layups also, considering standard deviation, with similar $E_{flex.}$ values between them (Table 4).

Despite its ability to withstand higher loads, LS configuration has shown an earlier severe loss of stiffness, while bioinspired laminates presented a progressive stiffness reduction before fail catastrophically. As may by observed in Figs. 7 and 8 b), HL and HL_S laminates presented a twist failure mode on the compression and tensile side that, under 3-PB loading conditions and according to Suksangpanya et al. [8] and Mencattelli and Pinho [10], typically onsets on 90° layers and grows throughout thickness by a matrix cracking manner. Moreover, this characteristic failure mode leads to larger displacements, which allows a higher energy absorption before a catastrophic failure takes place. Regarding LS configuration, as may be seen in Fig. 6 b), some layers failed catastrophically on compression side (top side on image) while on the tensile side (bottom side on image) layers integrity was kept and only some delaminations occurred. The higher number of undamaged plies orientated in 0° direction on the tensile side, conferred to this laminate a superior load bearing capability in comparison to HL and HL_S configurations.

Despite presenting also a partial twist failure mode and a lower fibre volume fraction, HYB layup has shown a higher load bending capability, under 3-PB solicitations, than both Bouligand-like configurations. This may be explained by higher number of plies orientated in 0° direction on the specimen tensile side.

As may be seen from ILSS load vs displacement curves in Fig. 4 b), all specimens have presented a plastic behaviour. This may be related to the rough and poorly defined interlaminar regions typically observed on LS, HL and HL_S laminates (see Fig. 5a)–c), respectively) and interlaminar resin rich interlaminar region of HYB configuration (see Fig. 5 d)). These morphological features, induced by vacuum bag infusion process, seem to redirect shear stresses to intralaminar regions, delaying interlaminar shear delaminations.

ILSS results have shown a similar apparent resistance to delamination of LS and HL layups, while a HL_S laminate has demonstrated a no significant reduction of this property. On the other hand, HYB configuration was the one that demonstrate a higher value of τ_{13}, as may be seen in Table 4.

The higher apparent global interlaminar resistance of HYB layup arrangement may be attributed to the lower fibre volume fraction observed during laminates characterization (Table 3). Its interlaminar resin richer region, that may be seen in Fig. 5 c), when compared to the other layup configurations (Fig. 5 a, b and c), seems to be responsible to improve the resistance to hold two adjacent plies. This is in good agreement with other experimental works, where it was observed a reduction of ILSS resistance with the increase of fibre volume fraction [27,28].

5. Conclusion

In this work, three new bioinspired carbon/epoxy laminates were proposed and manufactured by vacuum bag infusion. Additionally, a standard aircraft configuration (LS), produced in the same conditions, was taken as reference. All configurations were first characterised physically and morphologically and then according to three quasi-static mechanical tests, namely, tensile, long beam three-point bending and interlaminate shear strength.

From laminates characterisation, no significant differences in terms of thickness and fibre volume fraction were found between the reference (LS) and both Bouligand-like layups (HL and HL_S), however, the larger amount of weft threads on HYB laminate has led to a high presence of resin pockets, which resulted in a low fibre volume fraction and slightly higher thickness of this configuration. Moreover, no significant number of voids were found inside laminates, which confirms the suitability of vacuum bag infusion to produce these kinds of composite layups.

Quasi-static mechanical response of laminates was evaluated by tensile, three-point bending (3-PB) and interlaminar shear strength (ILSS) tests. From the experimental results and observations, it was concluded that:

- Under tensile conditions, all laminates have shown roughly the same Young's modulus (E) (40 GPa). However, all bioinspired configurations have revealed to fail at lower tensile stresses. On the other hand, while LS configuration has failed catastrophically, both Bouligand-like layups have shown a progressive failure mode.
- When compared to LS reference, under 3-PB testing conditions, both Bouligand-like configurations have revealed higher flexural moduli, whereas HYB layup has demonstrated a slightly reduction on this property. Moreover, all bioinspired configurations have developed translaminar failure mode, which lead to a lower load bearing capability, although larger displacements and higher energy absorption before catastrophic failure, while LS layup has shown a catastrophic failure in one of the 0° layers inside the laminate.
- Both Bouligand-like configurations have shown similar interlaminar shear strength as LS reference, while the larger amount of resin volume fraction has led to a superior performance of HYB layup. It was also observed a good corelation between finite element models and the failure mode of reference and both Bouligand-like arrangements, however, the large amount of weft threads in HYB seemed to play an important role on its failure mode.

Credit author statement

Luis Amorim: Conceptualization, Investigation, Writing - Original Draft, Visualization. Ana Santos: Conceptualization, Investigation, Writing - Original Draft, Visualization. João P. Nunes: Conceptualization, Writing - Review & Editing, Supervision. Júlio C. Viana: Conceptualization, Writing - Review & Editing, Supervision.

Declaration of competing interest

The authors declare that they have no known competing financial interests or personal relationships that could have appeared to influence the work reported in this paper.

Acknowledgments

This research was funded by the project "IAMAT—Introduction of advanced materials technologies into new product development for the mobility industries", with reference MITP-TB/PFM/0005/2013, under the MIT-Portugal program and in the scope of projects with references UIDB/05256/2020 and UIDP/05256/2020, exclusively financed by FCT—Fundação para a Ciência e Tecnologia. The authors also acknowledge PIEP (Centre for the Innovation in Polymer Engineering) for yielding of facilities and equipment.

Appendix A. Supplementary data

Supplementary data to this article can be found online at https://doi.org/10.1016/j.polymertesting.2021.107261.

References

[1] Y. Bouligand, Twisted fibrous arrangements in biological materials and cholesteric mesophases, Tissue Cell 4 (2) (1972) 189–217.
[2] S.N. Patek, R.L. Caldwell, Extreme impact and cavitation forces of a biological hammer: strike forces of the peacock mantis shrimp Odontodactylus scyllarus, J. Exp. Biol. 208 (19) (2005) 3655–3664.
[3] L. Cheng, L. Wang, A.M. Karlsson, Image analyses of two crustacean exoskeletons and implications of the exoskeletal microstructure on the mechanical behavior, J. Mater. Res. 23 (11) (2008) 2854–2872.
[4] Prilfish, Mantis Shrimp - Odontodactylus scyllarus," *Thailand Andaman Sea February 2008*, 2008 [Online]. Available: www.flickr.com. (Accessed 13 February 2020).
[5] T. Apichattrabrut, K. Ravi-Chandar, Helicoidal composites, Mech. Adv. Mater. Struct. 13 (1) (2006) 61–76.
[6] L. Cheng, A. Thomas, J.L. Glancey, A.M. Karlsson, Mechanical behavior of bio-inspired laminated composites Helicoidal structure, Compos. Part A 42 (2) (2011) 211–220.
[7] M.R. Abir, T.E. Tay, H.P. Lee, On the improved ballistic performance of bio-inspired composites, Compos. Part A Appl. Sci. Manuf. 123 (2019) 59–70. March.
[8] N. Suksangpanya, N.A. Yaraghi, R.B. Pipes, D. Kisailus, P. Zavattieri, Crack twisting and toughening strategies in Bouligand architectures, Int. J. Solid Struct. 150 (2018) 83–106.
[9] L. Mencattelli, S.T. Pinho, Realising bio-inspired impact damage-tolerant thin-ply CFRP Bouligand structures via promoting diffused sub-critical helicoidal damage, Compos. Sci. Technol. 182 (2019), 107684. June.
[10] L. Mencattelli and S. T. Pinho, "Ultra-thin-ply CFRP Bouligand bio-inspired structures with enhanced load-bearing capacity, delayed catastrophic failure and high energy dissipation capability," Compos. Part A Appl. Sci. Manuf., vol. 129, no. July 2019, p. 105655, 2020.
[11] L. Mencattelli and S. T. Pinho, "Herringbone-Bouligand CFRP structures: a new tailorable damage-tolerant solution for damage containment and reduced delaminations," Compos. Sci. Technol., p. 108047, 2020.
[12] L.K. Grunenfelder, et al., Bio-inspired impact-resistant composites, Acta Biomater. 10 (9) (2014) 3997–4008.
[13] J.S. Shang, N.H.H. Ngern, V.B.C. Tan, Crustacean-inspired helicoidal laminates, Compos. Sci. Technol. 128 (2016) 222–232.
[14] F. Pinto, O. Iervolino, G. Scarselli, D. Ginzburg, M. Meo, Bioinspired twisted composites based on Bouligand structures, Bioinspiration, Biomimetics Bioreplication 9797 (2016), 2016.
[15] D. Ginzburg, F. Pinto, O. Iervolino, M. Meo, Damage tolerance of bio-inspired helicoidal composites under low velocity impact, Compos. Struct. 161 (2017) 187–203.
[16] J.L. Liu, H.P. Lee, V.B.C. Tan, Failure mechanisms in bioinspired helicoidal laminates, Compos. Sci. Technol. 157 (2018) 99–106.
[17] J.L. Liu, H.P. Lee, V.B.C. Tan, Effects of inter-ply angles on the failure mechanisms in bioinspired helicoidal laminates, Compos. Sci. Technol. 165 (2018) 282–289. July.
[18] J.L. Liu, H.P. Lee, S.H.R. Kong, V.B.C. Tan, Improving laminates through non-uniform inter-ply angles, Compos. Part A Appl. Sci. Manuf. 127 (2019) 105625. July.
[19] J.L. Liu, H.P. Lee, K.S. Lai, V.B.C. Tan, Bio-inspired laminates of different material systems, J. Appl. Mech. 87 (3) (2020) 1–7.
[20] K. Autar, Kaw, *Mechanics Of Composite Materials*, second ed., vol. 29, Taylor & Francis, Inc., 2006.
[21] AT Nettles, Some examples of the relation between processing and damage tolerance, in: Proceedings 44th international SAMPE fall technical conference, Charleston, SC, October 2012, 22–25.
[22] H. Conway, B. Bancroft, D. Chebot, M. Devoe, C. Gouldstone, Impact resistance and residual strength of carbon fiber epoxy laminates with vertically-aligned carbon nanotube interfacial reinforcement, Int. SAMPE Tech. Conf. (2017) 1642–1651.
[23] Y. Cao, Z. Cao, Y. Zhao, D. Zuo, T.E. Tay, Damage progression and failure of single-lap thin-ply laminated composite bolted joints under quasi-static loading, Int. J. Mech. Sci. 170 (2020) 105360. December.
[24] N.A. Yaraghi, et al., A sinusoidally architected helicoidal biocomposite, Adv. Mater. 28 (32) (2016) 6835–6844.
[25] W. Ouyang, B. Gong, H. Wang, F. Scarpa, B. Su, H.X. Peng, Identifying optimal rotating pitch angles in composites with Bouligand structure, Compos. Commun. 23 (2021) 22–26, no. December 2020.
[26] N. Suksangpanya, N.A. Yaraghi, D. Kisailus, P. Zavattieri, Twisting cracks in Bouligand structures, J. Mech. Behav. Biomed. Mater. 76 (2017) 38–57. March.
[27] G. Mishra, S.R. Mohapatra, P.R. Behera, B. Dash, U.K. Mohanty, B.C. Ray, Environmental stability of GFRP laminated composites: an emphasis on mechanical behaviour, Aircraft Eng. Aero. Technol. 82 (4) (2010) 258–266.
[28] A. Mehndiratta, Analyzing variation in ILSS of fiber reinforced polymer laminates with respect to pressure variation in autoclave, MOJ Polym. Sci. 1 (3) (2017) 127–129.